PROCEEDINGS OF SCIENCE

Observational constraints on transient accelerators of ultra-high energy cosmic rays

Antonio Condorelli,[a,*] **Jonathan Biteau**[a] **and Olivier Deligny**[a]

[a] *Université Paris-Saclay, CNRS/IN2P3, IJCLab, 15 Rue Georges Clemenceau, 91405 Orsay, France*

E-mail: condorelli@ijclab.in2p3.fr

The primary population of extragalactic sources capable of accelerating ultra-high energy cosmic rays (UHECRs) is still unknown. We explore two generic hypotheses for tracing the density of UHECR sources in the Universe: we assume that the UHECR production rate follows the cosmic star formation rate density or stellar mass density. For each scenario, we infer a set of constraints for the emission mechanisms in the accelerators, for their energetics, and the abundances of elements at escape from their environments by fitting together the energy spectrum and the mass composition as measured by the Pierre Auger Observatory at energy above the so-called ankle ($10^{18.7}$ eV). From these constraints, we generate sky maps above 40 EeV expected from a catalog of more than 400,000 galaxies out to 350 Mpc, which provides a near-infrared flux-limited sample to map both stellar mass and star formation rate over the full sky. Considering a scenario of intermittent sources hosted in every galaxy, we show that the main features observed in the arrival directions of UHECRs can, in turn, constrain the burst rate of the sources, also considering the magnetic effects in the cosmic web. Local magnetic fields within a few Mpc could explain why no contributions are seen from past transients in the Magellanic clouds or the Milky Way while remaining visible from more distant galaxies. Finally, we compare the burst rate inferred in a transient scenario with astrophysical candidates. The comparison shows that the best candidates are long gamma-ray bursts with low luminosities and tidal disruption events.

38th International Cosmic Ray Conference (ICRC2023)
26 July - 3 August, 2023
Nagoya, Japan

*Speaker

© Copyright owned by the author(s) under the terms of the Creative Commons Attribution-NonCommercial-NoDerivatives 4.0 International License (CC BY-NC-ND 4.0).

PoS(ICRC2023)336

1. Introduction

The astrophysical objects which emit charged cosmic-ray particles at energies higher than 1 EeV remain elusive. However, the energy spectrum and mass composition of ultra-high energy cosmic rays (UHECRs) detected at the Pierre Auger Observatory over the last two decades have greatly constrained the emission mechanisms, source energetics, and abundances of elements in the source environment [1, 2]. According to the expectation that electromagnetic processes accelerate charged particles of atomic mass A to a maximum energy $E^{\max}_{Z_A}$, proportional to their electric charge, Z_A, the intensity of the individual nuclear components is expected to fall off at the same magnetic rigidity at the sources [3, 4]. This constraint derives mostly from the observed progressive increase with the energy of the mean logarithmic mass number $\langle \ln A \rangle$ [1]. The abundance of nuclear elements has been found being dominated by intermediate-mass elements ranging from He to Si, accelerated to $E^{\max}_{Z_A} \propto 5\ Z_A$ EeV and escaping the source environments with a very hard spectral index γ (considering the emission spectrum as $\frac{dN}{dE} \propto E^{-\gamma}$).

The production rate density of UHECRs is constrained to be on the order of $\mathcal{L} \simeq 10^{45}\,\mathrm{erg\,Mpc^{-3}\,yr^{-1}}$ to supply the observed energy density. Assuming that the UHECR luminosity of astrophysical sources is on the order of the electromagnetic luminosity, the value obtained for $\mathcal{L}$ can be used to identify the few classes of sources that emit light with a similar energy budget in the electromagnetic band [5]. Many candidates can, in fact, satisfy the energy constraints, ranging from sources feeding frequent occurring periods of electromagnetic emission with relatively low luminosity to catastrophic events of great luminosity occurring only very rarely.

From an observational point of view, sky maps of arrival directions support the view that UHECRs are primarily of extragalactic origin above the so-called ankle (5 EeV) [6]. They contain a possibly even larger depth of information that may resolve the degeneracy between common low-luminosity and rare high-luminosity source candidates matching the energetics requirements. The observed duration of a burst emitted as an instantaneous impulse grows with distance from the source in a rigidity-dependent manner for particles experiencing magnetic wandering throughout their propagation. As a result, the average number of visible bursting sources declines with energy much quicker than in a steady-state situation, and different burst rate densities should result in different sky maps.

The goal of this work is to complement existing limits on UHECR production rate density by using arrival directions to bracket the rate density of bursting sources. The fundamental idea of this research is that each galaxy in the flux-limited sample established by [7] may host transient periods of UHECR production at a given rate.

2. Description of the model

We use a near-infrared flux-limited sample to simulate the 3D distribution of galaxies [7], which maps both stellar mass ($M_\star$) and star formation rate (SFR) over the whole sky. The catalog contains around 400,000 galaxies; it provides unprecedented $M_\star$ and SFR cosmography within 350 Mpc, with a $50-50$ ratio of spectroscopic and photometric distances, as well as corrections for incompleteness as distance increases and Galactic latitude decreases. The distribution of galaxies within a 10 Mpc-width box in comoving supergalactic coordinates is compatible with a planar

PoS(ICRC2023)336

distribution along the Local Sheet [8]. The $M_\star$ distribution within a 600 Mpc-wide box is in good agreement with the 3D dark matter density fields inferred from Cosmic Flows (e.g. [9]). Finally, the catalogue provides incompleteness correction factors for the SFR density, which, like $M_\star$, converges to the deep-field value beyond 100 Mpc. We extend the $M_\star$ and SFR densities beyond 350 Mpc using the density model from [10]. In our model, each galaxy in the catalog is expected to contain UHECR sources that burst at a specific rate. For tracing the source emission, we examine two scenarios: $M_\star$ and SFR. In both scenarios, the observed intensity on Earth is influenced by each resolved galaxy within 350 Mpc and by the continuous density of unresolved galaxies beyond 350 Mpc.

The emission rate per energy unit of a single galaxy i is conveniently divided into the product of two components: the ejection rate of UHECRs and the number of particles per energy unit. This last term takes into account the shape of the injection spectrum, i.e. the exponentially-suppressed power-law function, as it provides a summary of the acceleration and ejection processes with a minimal number of parameters, namely the spectral indexes of protons and heavier nuclei (as in [11]), and the rigidity-dependent maximum energy. The emission rate is supposed identical at each source hosted by a galaxy. Individual galaxies are not further catalogued to high completeness and over a large portion of the sky beyond 350 Mpc. The ejection rate is then represented per energy unit and per comoving volume unit.

The all-particle energy spectrum measured on Earth receives contributions from the isotropic background (> 350 Mpc) and foreground sources of the catalog (≤ 350 Mpc), with the sum being over each detected species of mass number A. For our work, the Monte-Carlo package SimProp v2r4 [12] is used to calculate the extragalactic propagation.

Finally, to represent the probability density function of the direction of arrival given the location of the source in the direction $\mathbf{n}_i$, we use a von Mises-Fisher distribution centered on $\mathbf{n}_i$ with an adaptable concentration parameter, which is aimed at effectively modeling the magnetic deflections experienced by UHECRs throughout their propagation. This assumption is based on the idea that some directionality of the sources is preserved in the observed sky maps due to the high rigidity of the particles, which is a plausible hypothesis given the strength of the magnetic fields encountered. An accurate treatment of the deflections would necessitate detailed knowledge of the Galactic magnetic field as well as the structure and strength of the Local-Sheet magnetic field, both of which are expected to imprint random-type deflections from magnetic turbulence as well as mass-spectrometric ones from large-scale fields. Despite the most recent developments, such knowledge remains elusive. For this reason, we simulate deflections to first order using a single model parameter.

In a transient scenario, sources are only visible to an observer for a finite time, $\Delta\tau$, corresponding to the spread due to the magnetic fields along the line of sight. Because of the magnetic wandering of particles en route to Earth, the duration window is determined by the magnetic rigidity of the particles, the distance from the source, and the magnetic-field parameter values. The average number of fossil bursts, λ_i, that contribute to the energy spectrum observable now on Earth for an observation length substantially less than $\Delta\tau$ is

$$\lambda_i = \dot{k} M_{\star i} \Delta\tau. \tag{1}$$

with $\dot{k}$ expressed in $\mathrm{M}_\odot^{-1}\ \mathrm{yr}^{-1}$ units. Taking into account this relationship, the Poissonian nature of

PoS(ICRC2023)336

any transient scenario can be captured by drawing at random the number of source bursts in each galaxy.

In this work, the relevant magnetic fields that could play a role in the propagation of UHECRs have been taken into account, namely the Galactic magnetic field [$B_G \simeq 1$ μG, $\lambda_G = 100$ pc], the magnetic field in the Local Sheet [$B_{LS} = 0.5 - 25$ nG, $\lambda_G = 10$ kpc] and the extragalactic magnetic field [0.1 fG $\leq B_{EG} \leq$ 0.1 nG, $\lambda_G = 1$ Mpc]. All of them are considered for computing the angular spread and time spread expected for a particle of a given rigidity propagating through the Universe. For our investigation, the effect of UHECRs propagating in galaxy clusters is also taken into account: following [13], the transparency functions there provided are used to estimate the escaping fluxes from these environments. This has a great impact, especially on the Virgo cluster, the closest galaxy cluster to us ($d \simeq 16$ Mpc, $M \simeq 1.2 \cdot 10^{14}$ $M_\odot$) from which the Pierre Auger Collaboration does not see any indication of excess observed. Therefore, considering the confinement in the clusters is crucial to reproduce the observed sky maps [14].

3. Constraints on burst rate density from sky maps

3.1 Full-sky observations above 38 EeV

The Pierre Auger Observatory, located in the Mendoza province of Argentina and covering 3000 km^2, has been providing a study of the UHECR sky since 2004 with a total exposure of $\sim 122,000$ km^2 sr yr [15]. In parallel, the Telescope Array, located in Utah (USA) and covering 700 km^2, has been providing a view of the northern sky since 2008 with a total exposure of $\sim 18,000$ km^2 sr yr [16]. The full-sky map of arrival directions displayed in Fig. 1 has been produced as a consequence of several inter-collaborative efforts [17]. Despite the techniques for assigning energies to events being almost the same at both observatories, there are differences in how the primary energies are obtained. To create the sky map, the energy estimators are cross-calibrated to ensure that the intensities observed at each observatory are identical in the common field of view. As a result, the sky map includes events with energies greater than 38 EeV (49 EeV) in terms of the energy scale of the Pierre Auger Observatory (Telescope Array). For the sake of simplicity, we will refer to the energy threshold as 38 EeV from here on.

Due to propagation effect, the isotropic background of UHECR arrival directions produced by sources spread over the distant universe is reduced. The overdensities evidenced in Fig. 1 could potentially refer to dominating foreground sources in our area of the universe. Such excesses are only pieces of evidence at this stage as a blind search yields no statistically significant indications of anisotropy [14].

Even in the absence of compelling evidence for discrete sources, a link between UHECR arrival directions and the flux pattern of a class of astronomical objects might show an anisotropy that would trace the sources. A catalog of star-forming galaxies now provides the best evidence, with a confidence level of 4 σ against isotropy [17, 18]. In addition to verifying the arrival directions from the pre-defined positions of the galaxies, the clustering in UHECRs is tested by assigning a weight to each source candidate based on a proxy for its electromagnetic luminosity. The similarities between the model and the data are owing to overdensities around the supergalactic plane caused by galaxies in the Local Sheet. However, the signal strength, which is as low as $\simeq 10 - 15\%$, raises

PoS(ICRC2023)336

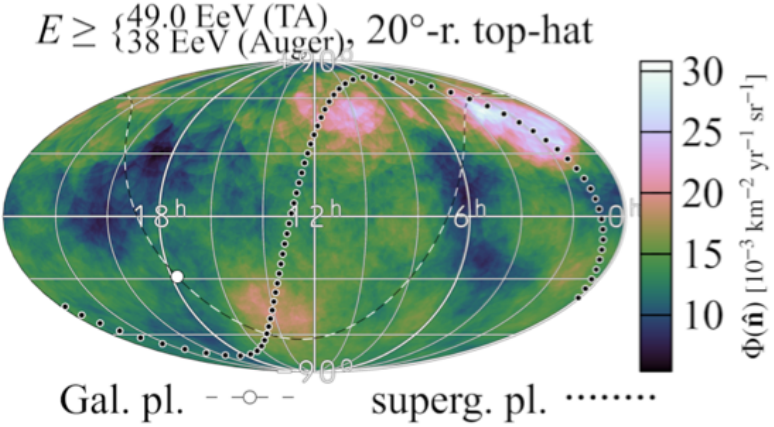

Figure 1: Flux map reconstructed at $E_{\text{Auger/TA}} > 38/49$ EeV. The dashed line indicates the Galactic plane and the dotted line the supergalactic plane. *Reproduced from [17].*

concerns. It precludes making clear conclusions regarding the acceleration of UHECRs simply in star-forming galaxies. The goal of the sky maps produced in the following sections is to investigate the rate of emission bursts in every galaxy that, given the measured angular scale of the correlation, may accommodate the reported signal-strength correlation.

3.2 Constraints on $\dot{k}$ from full-sky observations

According to Equation (1), for a given set of best-fit parameters to reproduce the energy spectrum and mass-composition data, the number of source bursts in each galaxy, n_i, can be drawn at random from a Poisson process with parameter λ_i, which is governed by $\dot{k}$ for a given setup of magnetic fields. The intensity of UHECRs detected on Earth above 38 EeV in each direction is then predicted, with the results based on a set of 100 random realizations for a given $\dot{k}$ value. Their median intensity above 38 EeV is shown in each direction in Figures 2 and 3. In comparison to mean sky maps, which simply represent the results obtained by weighting the burst rate of each galaxy by $\langle n_i \rangle = \lambda_i$, such median sky maps better reflect the stochastic nature of the transient-source scenario, i.e. the fact that bursts from nearby sources are not seen most of the time.

We begin with an analysis of the $\dot{k}$ range with a low value, $\dot{k} = 3 \cdot 10^{-17}$ $\text{M}_\odot^{-1}\text{yr}^{-1}$, in the left panel of Fig. 2. A low $\dot{k}$ value functions as a filter for sources situated within $\simeq$ 1 Mpc of the Milky Way. Indeed, the resulting burst rate is so low that it is quite likely that the burst episodes are short. Furthermore, the temporal dispersion induced in the magnetic field is insufficient to keep the contribution of the sources in this volume steady. As a result, the contribution of the Milky Way and relatively nearby galaxies, such as the Magellanic clouds or Andromeda, is suppressed in most realizations, and hence suppressed in the median sky map. This phenomena also applies to galaxies between 1 and 10 Mpc to some extent; however, the contributions of galaxies such as M81/82, M51/106, Maffei1 and NGC253 are not completely suppressed but rather attenuated due to the temporal dispersion that compensates for the smallness of $\dot{k}$. Beyond 10 Mpc, the rise in the number of sources and the temporal spread combine to produce a very stationary image of the galaxies towards the Laniakea, Perseus-Pisces and Shapley superclusters, despite the smallness of

PoS(ICRC2023)336

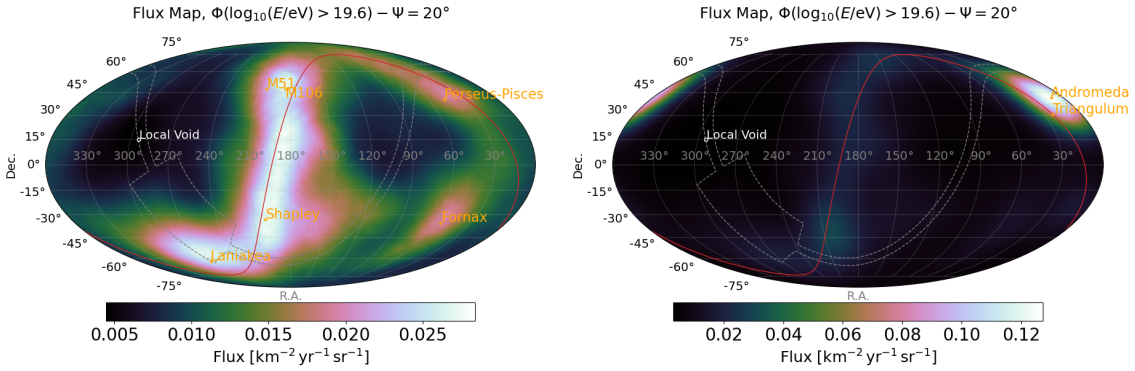

Figure 2: Left panel: Sky map of the expected flux above $E_{\rm th} = 10^{19.6}$ eV considering $\dot{k} = 3 \cdot 10^{-17}$ $M_{\odot}^{-1} yr^{-1}$. Right panel: Sky map of the expected flux above $E_{\rm th} = 10^{19.6}$ eV considering $\dot{k} = 10^{-14}$ $M_{\odot}^{-1} yr^{-1}$. In both cases a burst rate following the stellar mass density is considered. A 20 top-hat smoothing is adopted as in Fig. 1.

$\dot{k}$. Overall, a value of $\dot{k} = 3 \cdot 10^{-17}$ $M_{\odot}^{-1}$ yr^{-1} produces obvious differences between the model and the data and should be avoided.

A much larger value of $\dot{k}$, such as $\dot{k} = 10^{-14}$ $M_{\odot}^{-1}$ yr^{-1} implies other, equally noticeable dissimilarities, as shown in the right panel of Fig. 2. In such a scenario, the resulting rate of bursts is large enough to indicate contributions from extremely close sources, particularly Andromeda, in the majority of realizations. Increasing the value of $\dot{k}$ would even allow the Milky Way to dominate the total intensity. As a result, high $\dot{k}$ values can also be disregarded.

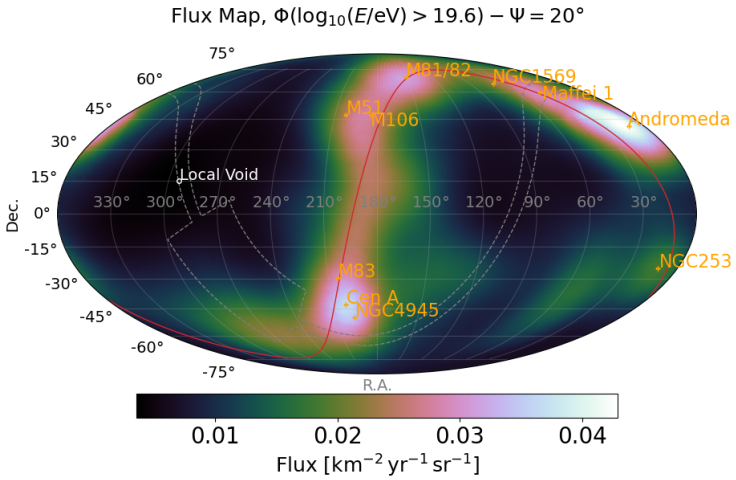

Figure 3: Sky map of the expected flux above $E_{\rm th} = 10^{19.6}$ eV considering $\dot{k} = 1 \cdot 10^{-15}$ $M_{\odot}^{-1} yr^{-1}$. A 20 top-hat smoothing is adopted as in Fig. 1.

The investigation of extreme values described above thus brings up the prospect of bracketing the likely values of $\dot{k}$. A scan of uniformly distributed values in decimal logarithm was performed for this purpose. The best similarities are found for values of $\dot{k} \in [10^{-16}, 3 \cdot 10^{-15}]$ $M_{\odot}^{-1}$ yr^{-1} that allow the contributions of galaxies from the Council of Giants (Centaurus A, NGC 4945, M83,

PoS(ICRC2023)336

NGC 253), from M51/106 and Andromeda to dominate. The median sky map produced with $\dot{k} = 1 \cdot 10^{-15}$ $M_{\odot}^{-1}$ yr^{-1}, shown in Fig. 3, allows us to appreciate the similarities with the data.

The above results are obtained for magnetic field amplitudes in the Local Sheet ranging from 10 to 25 nG. Smaller amplitudes, which lie at the low end in large-scale structure simulations [19], would not allow for the generation of sky maps similar to those displayed in Fig. 3. This is because the time spread $\Delta\tau$ experienced by particles coming from the Council of Giants would be comparable to that encountered by particles originating from galaxies in the Local Group (Magellanic clouds, Andromeda, and so on). In such a circumstance, the contribution of the Council of Giants, which is needed to reproduce the data, would be largely outweighed by that of very local galaxies for a high rate of bursts, while it would be dominated by more distant sources for a low rate of bursts. Magnetic field amplitudes in the Local Sheet greater than $\simeq 25 - 30$ nG, on the other hand, would lead to spreads in the UHECR arrival directions inconsistent with those found in Fig. 1. As a result, magnetic field amplitudes in the Local Sheet between 10 and 25 nG are favored.

4. Constraining on the source populations

The combined fit of spectrum and composition put constraints on the emissivities of UHECR sources [11]; among the plausible stellar-sized candidates which fulfill the energetic requirements, we report in Figure 4 the burst rate of core-collapse supernova (CC-SN [20]), CC-SN of type Ib/c [21], low luminosity long gamma-ray burst (LL-lGRB [21]), high luminosity long gamma-ray burst (HL-lGRB [21]) and tidal disruption event (TDE [22]). The burst rate required to match the measured arrival direction map is shown as a gray band. We conclude that both low luminosity long gamma-ray bursts and tidal disruption events are suitable candidate UHECR sources in a transient scenario.

Similar studies dedicated to other types of transient or intermittent sources, such as jetted AGN, should further shed light on the few remaining candidates for UHECR acceleration.

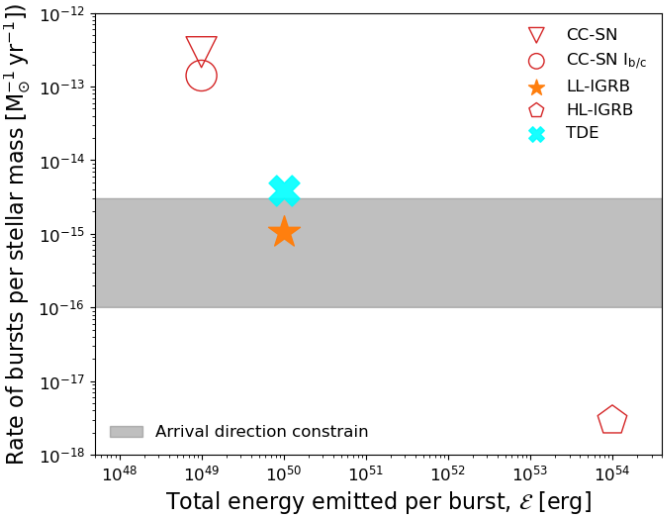

Figure 4: Constraints on $\dot{k}$ and in a $M_{\star}$ scenario (gray band). Source candidates are shown as markers.

PoS(ICRC2023)336

5. Aknowdlegements

The authors gratefully acknowledge funding from ANR, via the grant MultI-messenger probe of Cosmic Ray Origins (MICRO), ANR-20-CE92-0052.

References

[1] Aab, A. & al., *Phys. Rev. D*. **90**, 122005 (2014).

[2] Abreu, P. & al., *Eur. Phys. J. C*. **81**, 966 (2021).

[3] Aloisio, R., Berezinsky, V. & Blasi, P., *JCAP*. **10** pp. 020 (2014).

[4] Aab, A. & al., *JCAP*. **4** pp. 038 (2017), [Erratum: JCAP 03, E02 (2018)].

[5] Batista, R., & al., *Frontiers In Astronomy And Space Sciences*. **6** (2019,6).

[6] Aab, A. & al., *Science* **357**, 1266-1270 (2017).

[7] Biteau, J., *Astrophys. J. Supp.*. **256**, 15 (2021).

[8] McCall,M., *Mon. Not. Roy. Astron. Soc.*. **440**, 405-426 (2014).

[9] Hoffman, Y., Pomarede, D., Brent Tully, R. & Courtois, H. *Nat Astron*., 0036 (2017,2).

[10] Koushan, S. & al., *Mon. Not. Roy. Astron. Soc.*. **503**, 2033-2052 (2021)

[11] Luce, Q., Marafico, S., Biteau, J., Condorelli, A. & Deligny, O. *Astrophys. J.*. **936**, 62 (2022).

[12] Aloisio, R., Boncioli, D., Di Matteo, A., Grillo, A., Petrera, S. & Salamida F., *JCAP*. **11** 009 (2017).

[13] Condorelli, A. , Biteau, J. and Adam, R., submitted to *Astrophys. J.* (2023).

[14] Abreu, P. & al., *Astrophys. J.*. **935**, 170 (2022).

[15] Aab, A. & al.,*Nucl. Instrum. Meth. A*. **798** pp. 172-213 (2015).

[16] Abu-Zayyad, T. & al., *Nucl. Instrum. Meth. A*. **689** pp. 87-97 (2013).

[17] Di Matteo, A. & al., *PoS*. **ICRC2021** pp. 308 (2021).

[18] Aab, A. & al., *Astrophys. J.*. **853**, L29 (2018).

[19] Vazza, F., Brüggen, M., Gheller, C., Hackstein, S., Wittor, D. & Hinz, P., *CQG*. **34**, (2017,12).

[20] Madau, P. & Dickinson, M., *Annual Review Of Astronomy And Astrophysics*. **52**, 415-486 (2014,8).

[21] Liu, R., Wang, X. & Dai, Z.,*MNRAS* **418**, 1382-1391 (2011,12).

[22] Khabibullin, I. & Sazonov, S.,*MNRAS*. **444**, 1041-1053 (2014,8).

PoS(ICRC2023)336